Volume 1 | Number 1 | Jan 2013 | Pages 1–100

Nanoscale

www.rsc.org/nanoscale

ROYAL SOCIETY OF CHEMISTRY

ROYAL SOCIETY OF CHEMISTRY

www.rsc.org/nanoscale

Journal Name

COMMUNICATION

A Highly Dense Graphene-Sulfur Assembly: A Promising Cathode for Compact Li-S Batteries

Chen Zhang, [‡ab] Dong-Hai Liu, [‡ab] Wei Lv, [c] Da-Wei Wang, [*d] Wei Wei, [ab] Guang-Min Zhou, [e] Shaogang Wang, [e] Feng Li, [e] Bao-Hua Li, [c] Feiyu Kang, [c] Quan-Hong Yang [*abc]

This work reports the highly dense graphene/sulfur assembly for compact Li-S batteries with high volumetric capacity, while retaining the good structural stability and conductivity. This dense assembly was prepared by a reduction-triggered self-assembly of graphene oxide with simultaneously deposition of sulfur followed by a unique evaporation-induced spatially volume shrinkage. Such a novel assembly has an ultrahigh density, delivering an unprecedented high volumetric capacity that is much higher than common carbon/sulfur cathodes. In particular the unique spatial confinement derived from the shrinkage of graphene/sulfur assembly is favorable for the stabilization of sulfur cathodes.

High performance compact energy storage devices are of increasing significance to satisfy the urgent demand for advanced portable electronics.[1-4] Therefore, great advances have been made to fabricate electrode materials with high volumetric capacity and to develop devices with a high volumetric energy density, which is essential for next-generation batteries.[5-7] Among many post-lithium-ion technologies, lithium-sulfur (Li-S) batteries are of particular importance on account of their high specific energy density (2600 Wh kg^{-1}), low cost and environmental friendliness.[8-10] Sulfur, which is electrochemically active, has been demonstrated as a promising cathode candidate (theoretical specific capacity: 1675 mAh g^{-1}, almost 10 times higher than that of LiFePO$_4$) to substitute for traditional cathode materials for the purpose of achieving a higher energy density. Since a sulfur cathode is insulating and electrochemically unstable, carbon-sulfur hybrids have been deployed to overcome these obstacles.[9] However, there is a huge gap between the volumetric capacity of a state-of-the-art sulfur-carbon cathode and the theoretical value of pure sulfur (3467 mAh cm^{-3}),[2, 11] thus hindering the development of highly compact Li-S batteries.

Generally, the use of carbon materials is essential to improve the conductivity of the sulfur cathode, and the porous structure of carbon can tackle the shuttle effect, leading to a better utilization of sulfur.[12-14] Nonetheless, porous carbons usually have a low density (in most cases, 0.3~ 0.6 g cm^{-3}) and the sulfur loading is always restricted to low values to ensure satisfactory performance.[15] These factors result in the low density of carbon/sulfur cathodes unless the nano-texture is appropriately tailored.[14] Such a low density causes

the low volumetric energy density of packed Li-S batteries, further hindering the advance to compact applications. In other cases the use of nano-sized sulfur with high electrochemical performance sacrifices the volumetric capacity due to the low packing density.[16] Therefore, exploring an effective solution to the low volumetric capacity of the sulfur cathode is urgently required, and the key is to construct novel carbon-sulfur assemblies, which combine both excellent electrochemical performance and high density.

One solution is to use bulk sulfur for the cathode or to increase the sulfur content up to 90 wt % in the C-S hybrid. But the obvious drawback is that the cathode conductivity is poor because of the dominant insulating sulfur, and this will eventually harm the electrochemical efficiency. Another more practical solution is to use a porous, yet very dense, carbon host, which guarantees a highly packed nanostructure that also limits the shuttle effect and provides fast ion and electron transport. Graphene is believed to be an ideal building block for constructing various carbon nanostructures due to its flexible sheet-like structure. Unfortunately such a graphene-based assembly is usually very light.[17-20] Significant breakthroughs in assembling highly dense graphene materials were made only very recently (1.33~ 1.58 g cm^{-3}).[6, 7] Our group and Li's group have reported the extraordinary volumetric capacitance of these novel super-dense graphene-derived electrodes prepared by the assembly of reduced graphene oxide (rGO).[6, 7] Thus, we believe that these novel super-dense graphene assemblies are promising platforms for constructing high-density sulfur-based cathode materials with superior volumetric capacity. However, sulfur intrusion into these highly dense carbons by a traditional melt impregnation approach (thermal or solution-based) is very challenging and inefficient due to the restricted access to the tortuous small pores they contain. Based on the success of our evaporation-induced drying (EID) strategy for the synthesis of a highly dense graphene monolith, we have extended EID to the synthesis of a highly dense graphene/sulfur monolith. The idea was to prepare a graphene/sulfur hydrogel, which is subsequently submitted to EID for strong volume contraction. Since the sulfur is pre-loaded onto the graphene sheets, post-EID sulfur intrusion is unnecessary.

In a previous study, we have demonstrated that H$_2$S with an ultrahigh sulfur content (94 wt %) is an excellent reducing agent for GO and the resulting hybrid shows appealing performance as an

electrode in Li-S batteries.[21] However, its low density is unsatisfactory because it provides neither a high volumetric capacity nor strong confinement of polysulfides. The new strategy involves the pre-deposition of sulfur on the surface of the graphene sheets which allows us to obtain a highly dense but porous graphene-sulfur hybrid structure if such hybrid sheets can be compactly assembled. Here we report the increased volumetric capacity of a highly dense rGO/sulfur assembly (HDGS) prepared by evaporation-induced drying a hydrogel consisting of rGO/sulfur sheets. The rGO/sulfur hydrogel is formed by a room temperature reduction-induced assembly, which requires balanced amounts of rGO and sulfur. HDGS is featured by the highly shrunken and nonporous texture, which is critical for high volumetric performance.

H_2S is irreplaceable in the preparation of HDGS since it serves both as the reducing agent to trigger the self-assembly and as the sulfur source, as illustrated in **Fig 1a**. Typically, H_2S was used as the reducing agent to realize the reduction of GO and the loading of sulfur simultaneously, further accelerating the self-assembly of the rGO/S sheets. During the drying, rGO sheets uniformly decorated with sulfur spontaneously assembled into a cylindrical 3D monolith and the dispersion became transparent indicating the removal of the dispersed rGO/S sheets. It should be noted that totally different products (a 3D assembly or a powder precipitate) are formed depending on the reduction degree of the GO by the H_2S. To obtain a well-shaped 3D assembly, the reduction period needs to be optimized because rGO sheets will spontaneously interconnect upon
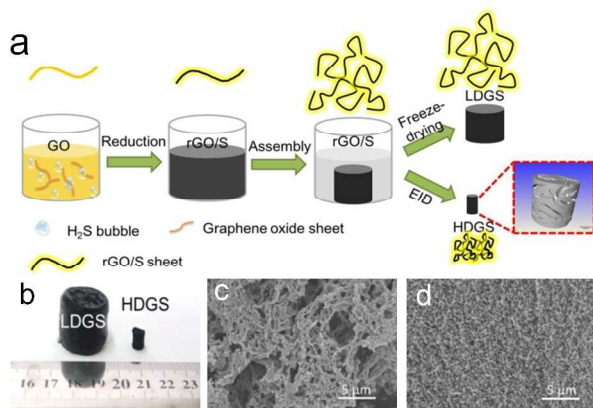

Fig 1. (a) Illustration of the formation of HDGS and LDGS. (b) Optical photos of LDGS and HDGS. SEM images of (c) LDGS and (d) HDGS.

transition from fully hydrophilic (before reduction) to partially hydrophobic (after reduction). A shorter reaction cannot lead to a sufficient reduction of GO, while a prolonged reaction will induce an excessive hydrophobic nature (**Fig S1**, from the Raman spectra), both of which make the assembly of a well-shaped 3D structure difficult. This phenomenon is consistent with the reported self-assembly of graphene oxide owing to the removal of hydrophilic oxygen groups.[22-24] Therefore, an optimized reduction time of 60 min is used in this work. And the subtle control of the reaction time induces totally different macroscopic and microstructural morphology although the other parameters are almost the same. We compared different drying processes of the same rGO/S hydrogel to tune the density of the resulting assemblies. HDGS (apparent density: 1.53 g cm^{-3}) was obtained only using EID, while a foam-like low density rGO/S assembly (LDGS, apparent density: 0.06 g cm^{-3}) was prepared by a freeze-drying method (Fig 1b). It can be clearly observed that the LDGS has a cylindrical shape, which inherits the shape and volume of the original rGO/S hydrogel. But during EID (vacuum drying at room temperature), the cylindrical hydrogel

gradually shrank and finally turned into a very hard cylindrical monolith. It should be noted that in the whole drying process, only water evaporation accounted for the weight loss; there was no substantial loss of rGO/S sheets, and this method does not damage the intrinsic microstructure of the 3D hydrogel but introduces a high density. This means that all the rGO/S sheets in the as-prepared hydrogel are confined and packed into a much smaller volume, leading to a dramatic density increase and a decrease of the pore size for the HDGS. In the case of LDGS, fast freezing and sublimation of the ice does not cause a collapse or shrinkage of the microstructure of the hydrogel [25] so that the material obtained has a lower density and is more porous than HDGS. Scanning electron microscopy (SEM) images (Fig 1c and 1d) further demonstrates the totally different microstructure between LDGS and HDGS. Macropores of up to several microns can be observed in LDGS while no large pores are identified in HDGS at low magnification. It can be clearly seen that the interconnected rGO/sulfur sheets formed a tightly-knit structure and are accommodated in a very limited space. Neither micropores nor mesopores can be identified from the SEM or the X-ray diffraction microtomography (XRD CT, Fig 1a) due to the small pore size.[26] X-ray diffraction (XRD) patterns further indicate the effective reduction of GO from the disappearance of the low angle peak at about 12° (**Fig 2a**). Long-range stacking of graphene layers is not observed as evident from the lack of a strong diffraction peak at around 26° (Fig 2a). Considering the significant volume shrinkage in HDGS, it is likely that the rGO/sulfur sheets were highly wrinkled so as to pack into tiny spaces without restacking face-to-face. Even after the severe shrinkage of the rGO/sulfur hydrogel, sulfur cannot
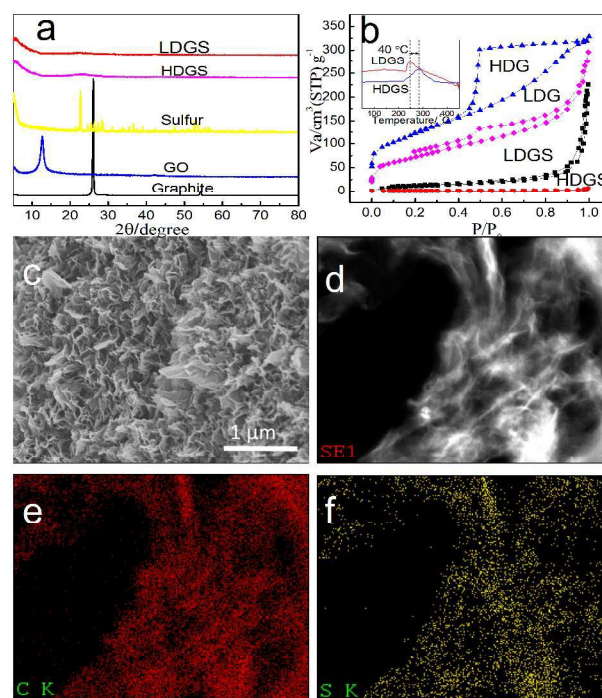

Fig 2. (a) XRD patterns of graphite, graphite oxide, sulfur, LDGS and HDGS. (b) N_2 adsorption isotherms of LDGS, HDGS, LDG and HDG, inset are DSC curves of LDGS and HDGS. (c) Magnified SEM image of HDGS. (d) Dark field image of HDGS. Elemental maps of (e) carbon and (f) sulfur.

be detected in the XRD patterns. This suggests the sulfur produced through the *in-situ* oxidation of H_2S by oxygen groups on pristine GO sheets exists as ultrafine particles.[27] To further evaluate the microstructure of HDGS, electron microscopy (SEM, TEM) and N_2-

adsorption/desorption isotherms were used to analyze its texture and pore structure. Higher magnification SEM images of HDGS reveal a clear porous structure in the HDGS cross-section. TEM (Fig 2d-f) observation further confirms that HDGS has a similar, albeit much smaller, pore structure to LDGS. Elemental mapping of C, O and S accompanied by dark-field images of HDGS show a well-matched spatial distribution of these elements, and such a uniform distribution of sulfur is favorable for its application in a Li-S battery. N_2 adsorption behavior shows that LDGS has a type-III isotherm, which is mostly attributed to the large mesopores and macropores formed by the interconnected graphene sheets. No obvious micropores can be identified, and a specific surface area of 49 m^2 g^{-1} is estimated from Brunauer-Emmett-Teller (BET) calculations. The adsorption amount of N_2 adsorbed by HDGS at high pressures is much less than that of LDGS due to the decrease in the amount of macroporosity caused by the volume shrinkage. However the amount adsorbed at low pressures did not increase as expected mainly because of the uniform surface coverage of graphene by sulfur that blocks the entrance of N_2 to the small pores in the HDGS. To clarify the distinct porous structure of HDGS and LDGS and obtain further insight into how the graphene sheets accommodate sulfur, both LDGS and HDGS were heated at 300 ºC for 6 h to evaporate the attached S leaving the bare graphene skeleton without any structure collapse. Compared with the isotherm of LDGS, it is obvious that the isotherm of HDGS after the removal of S (HDG) was transformed into a combination of type II and IV isotherms with a dramatic increase of adsorption at low pressures and the appearance of a wide and pronounced hysteresis loop, which is always indicative of the "ink bottle-like" mesopores in HDG. These ink bottle-like pores are defined as pores consisting of wide bodies with narrow necks, which are similar to "Shiu mai" with graphene skin and sulfur stuffing (**Fig S2**).[28-30] It is quite interesting that such a structure may improve the confinement of sulfur and polysulfides but Li$^+$ can move freely through the open neck. In order to better understand the confinement effect of HDGS and LDGS, DSC measurements were conducted in a N_2 atmosphere (Fig 2b). The peak temperature for the evaporation of sulfur from HDGS is much higher (40 °C) than that for LDGS, indicating a stronger confinement of sulfur by HDGS.[31, 32] The isotherm of LDG after the removal of S from LDGS has the same shape as the LDGS with a slightly increased adsorption amount. This is attributed to the open macroporous structure with very large pores, which does not change even after loading with sulfur. The N_2 adsorption behavior indicates that the use of different drying process induced totally different morphologies and microstructures of the 3D graphene assembly, and HDGS has a peculiar pore structure that makes it suitable for the sulfur cathode. The comparison of the pore volume and surface area is illustrated in Table S1.

The sulfur content in HDGS is estimated to be 32 wt % by elemental analysis (combustion method, see Table S2), which is slightly lower than in our previous work due to the shorter reaction time.[21] During drying, sulfur is closely attached to the graphene sheets and no aggregation occurs during the volume shrinkage. Raman spectra also showed no S vibration signal in the range of 100-500 cm^{-1}, implying the ultrafine particle/crystal size of sulfur in HDGS (**Fig S1**).[5, 27] The degree of reduction of the GO is also critical for the electrochemical performance since the restoration of the sp^2 network can effectively improve the electrode conductivity. XPS analysis was conducted to probe the chemical state of each element, and detailed peak analysis of C_{1s} indicates reduction of GO by H_2S (**Fig S3**).[33] The electrical conductivity of a HDGS monolith was measured by a I-V curve using an electrochemical workstation (**Fig S4**), and it is interesting that even after the incorporation of S, the conductivity (about 30 S m^{-1}) is of the same order of the similar

carbon free of sulfur loading,[7] revealing that the compact structure is favorable for electron transfer. From the computed image (XRD CT) of the test slice shown in Fig 1a, neither porous structure nor sulfur phase can be distinguished in this HDGS image due to the limited object size, in agreement with the XRD and Raman results.

3D graphene-based C/S materials have been demonstrated as promising cathode materials for the Li-S battery.[12] In this communication, the high volumetric capacity for HDGS compared with LDGS is highlighted due to the improved density of the carbon-based materials, demonstrating the potential of this approach for Li-S batteries with an excellent volumetric energy density. Cyclic voltammetry (CV) was used to elucidate the electrochemical process of the HDGS in the voltage range of 1.5-3.0 V at a sweep rate of 0.1 mV s^{-1}, as shown in **Fig 3a**. In the first cycle, the cathodic peaks located at 2.30 and 2.05 V are attributed to the reduction of S to high-order polysulfide followed by a subsequent reduction to insoluble discharge products Li_2S. Oxidation peaks can be identified in the anodic scan and are typical of the transformation of lithium sulfide to polysulfides and sulfur. The CV behavior is similar to
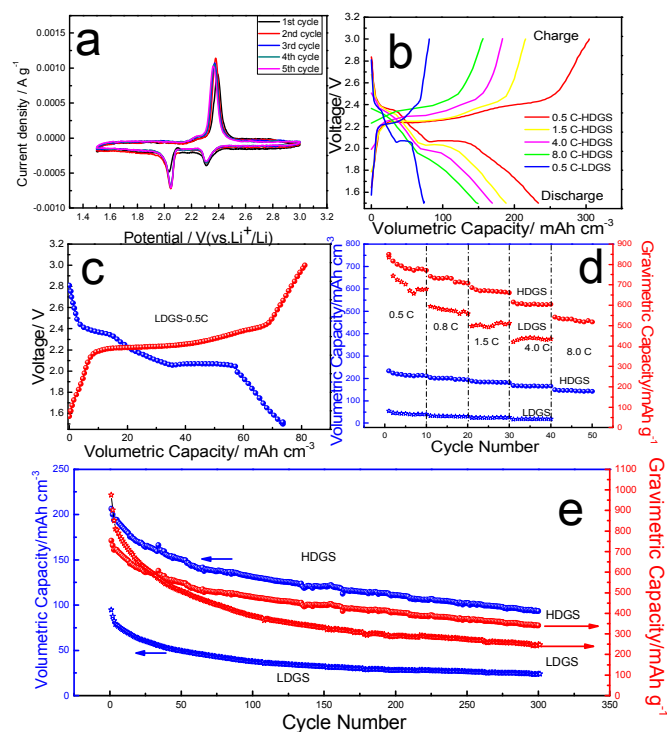

Fig 3. (a) CV curves of the first 5 cycles for HDGS at a scan rate of 0.1 mV s^{-1}. (b) Charge-discharge profiles of HDGS and LDGS at different rates. (c) Charge-discharge profile of LDGS at 0.5 C. (d) Rate performance of HDGS and LDGS. (e) Cycle performance of HDGS and LDGS.

related reports, demonstrating the effective incorporation of sulfur and its possible use in a Li-S battery.[34] The CV curves remained stable after the first cycle, also suggesting a relatively stable cyclic performance. Fig 3b shows the galvanostatic charge-discharge curves of HDGS at different current densities of 0.5, 1.5, 4.0 and 8.0 C, and also shows the curve of LDGS at 0.5 C. To better highlight the benefit of the highly dense structure of HDGS, we used the volumetric capacity of the electrode materials as the main evaluation parameter, and the packing densities of the prepared cathode are 1.07 and 0.38 g cm^{-3} for HDGS and LDGS, respectively. It should be noted that even difference between the density of HDGS and LDGS

decreased from 26 time to 3 times after the fabrication of electrode pallet, the packing density of HDGS is still much higher than of LDGS, suggesting the potential of our proposed strategy. From the charge-discharge curves, it can be seen that the charge and discharge plateaus correspond well to the CV results, and even at a current density of 4.0 C, the shape and plateau did not change significantly, revealing the good stability of HDGS at a high rate. A higher rate of 8.0 C is further used to examine the material's ultrahigh charge-discharge behavior, and the curves show a more prominent polarization than at lower rates, but a typical charge-discharge curve with distinct plateaus is recovered when the current density is switched back to 0.5 C after being subjected to the high rate of 8.0 C, indicating a structural and electrochemical stability during the high rate charge-discharge (**Fig S5**). Charge-discharge curves of LDGS at 0.5 C are also shown in Fig 3b, the plateaus are clearly observed even with a much smaller volumetric capacity. A magnified curve in Fig 3c further indicates the similar electrochemical plateaus of LDGS even though its volumetric capacity is almost 3 times lower.

The rate capability of HDGS is also measured by the coin cell configuration shown in Fig 3d. HDGS can deliver a volumetric capacity of 233 mAh cm^{-3} at 0.5 C, and after charge-discharge under different rates with 10 cycles for each rate, a capacity of 169 mAh cm^{-3} can be retained (capacity retention of 73%) at 4.0 C and 149 mAh cm^{-3} (capacity retention of 64%) at 8.0 C, illustrating an excellent rate performance. Moreover, HDGS recovered its capacity to around 164 mAh cm^{-3} with regenerated charge-discharge plateaus when the current density was restored to 0.5 C, implying the structure of the sulfur electrode remains stable after being subjected to intense charge-discharge. Compared with LDGS, HDGS has even a slightly better rate performance despite its totally different volumetric capacity. The high rate performance is attributed to the tightly interconnected rGO/sulfur sheets, which provide faster electron transfer channels due to their intimate contact. The abundance of micro- and meso-pores is also favorable for ion transport during the charge-discharge process.[35] More importantly, except for the good rate performance, the compact structure can provide an excellent shield for sulfur that hinders the dissolution of polysulfides, resulting in improved cycle stability. The cycle performance was evaluated to confirm the benefits of this structure and a capacity retention of around 45% is achieved after 300 cycles at a rate of 0.8 C with a capacity fade of 0.18% per cycle, which is better than for LDGS with a rapid capacity fade upon cycling (retention of 25% after 300 cycles with a capacity fade of 0.23% per cycle). The different cycle stability is due to the totally different microstructure. The open and large pore structure of LDGS allows barrier-free transport of ions at the cost of a lack of effective spatial confinement for the polysulfides, while the tightly interconnected graphene sheets and the abundant ink-bottle-like mesopores provide ideal accommodation for sulfur and the polysulfides. The Coulombic efficiency of HDGS is higher than that of LDGS after the first cycle, especially for a prolonged cycling, indicating a better confinement due to the better structural stability (Fig. S6). Electrochemical impedance spectroscopy (EIS) measurements of HDGS and LDGS are shown in Fig. S7. The internal resistance of HDGS electrode is about 3.5 ohm, which is lower than that of LDGS electrode, indicating a higher conductivity. The charge-transfer resistance Rct of HDGS and LDGS are estimated to be around 24 ohm and 58 ohm respectively. The much smaller Rct also indicates the faster charge transfer process in electrochemical reaction, resulting in a better rate performance. It is notable that despite the different rate and cyclic performances of HDGS and LDGS, totally different volumetric capacities of almost 4 times are estimated while their gravimetric capacities are almost the same. Such a distinguished high volumetric capacity for HDGS is ascribed to its fine microstructure. Compared

with Zhang's study,[14] our strategy focuses on the design of materials structure rather than improving the sulfur content for achieving a high volumetric performance. Even with a relatively low sulfur content (32 %), the HDGS still delivers a comparable volumetric capacity to the CNT/sulfur composite with a higher sulfur content of 54 %,[14] indicating the potential of our proposed strategy. But frankly speaking, there is still long distance between the volumetric capacities of HDGS and CNT/sulfur with 90% sulfur proposed by Zhang.[14] Thus a higher sulfur content is necessary to further improve the volumetric capacity of our materials. It can be predicted that our strategy is versatile to achieve a high volumetric capacity only with a moderate sulfur content due to the well-designed dense structure, which guarantees the conductivity and utilization of sulfur. Some efforts to improve the sulfur content in HDGS is being made, and the binder and current collector-free slice of HDGS is also being investigating as a model electrode for future applications.

In summary, a 3D graphene/sulfur assembly with high density and an almost nonporous structure was fabricated by combining reduction-triggered assembly and evaporation-induced drying. We have demonstrated a very high volumetric capacity of this highly dense cathode that is of obvious potential for applications in compact Li-S batteries. The presence of the sulfur in the unique ink-bottle shaped pores in HDGS is good for the confinement of both the sulfur and polysulfides formed, resulting in both good rate capability and cycle performance. In stark contrast, we show that without a highly dense structure, the volumetric capacity can be 3 times lower regardless of having the same rGO/sulfur sheets as building blocks. This further indicates that our evaporation-induced drying is an effective way for the construction of sulfur-based cathode materials to achieve a high volumetric energy density in Li-S batteries, although the sulfur content needs to improve in our case. It is expected that such a unique dense structure may be beneficial for the improvement of the volumetric energy density of many other energy storage devices.

Acknowledgements

Notes and references

[a] Key Laboratory for Green Chemical Technology of Ministry of Education, School of Chemical Engineering and Technology, Tianjin University, Tianjin 300072, China. _qhyangcn@tju.edu.cn_

[b] Collaborative Innovation Center of Chemical Science and Engineering, Tianjin 300072, China.

[c] Engineering Laboratory for Functionalized Carbon Materials, Graduate School at Shenzhen, Tsinghua University, Shenzhen 518055, China.

[d] School of Chemical Engineering, UNSW Australia (The University of New South Wales), Sydney, NSW 2052, Australia. _da-wei.wang@unsw.edu.au_

[e] Shenyang National Laboratory for Materials Science, Institute of Metal Research, Chinese Academy of Sciences, Shenyang 100016, China.

‡These two authors are equal main contributors

1.   C. Liu, F. Li, L. P. Ma and H. M. Cheng, _Adv. Mater._, 2010, **22**, E28-E62.

2.   P. G. Bruce, S. A. Freunberger, L. J. Hardwick and J. M. Tarascon, *Nat. Mater.*, 2012, **11**, 19-29.
3.   A. S. Arico, P. Bruce, B. Scrosati, J. M. Tarascon and W. Van Schalkwijk, *Nat. Mater.*, 2005, **4**, 366-377.
4.   H. Nishide and K. Oyaizu, *Science*, 2008, **319**, 737-738.
5.   G. M. Zhou, D. W. Wang, F. Li, P. X. Hou, L. C. Yin, C. Liu, G. Q. Lu, I. R. Gentle and H. M. Cheng, *Energy Environ. Sci.*, 2012, **5**, 8901-8906.
6.   X. W. Yang, C. Cheng, Y. F. Wang, L. Qiu and D. Li, *Science*, 2013, **341**, 534-537.
7.   Y. Tao, X. Y. Xie, W. Lv, D. M. Tang, D. B. Kong, Z. H. Huang, H. Nishihara, T. Ishii, B. H. Li, D. Golberg, F. Y. Kang, T. Kyotani and Q. H. Yang, *Sci Rep*, 2013, **3**, 2975.
8.   A. Manthiram, Y. Z. Fu and Y. S. Su, *Accounts Chem. Res.*, 2013, **46**, 1125-1134.
9.   D. W. Wang, Q. C. Zeng, G. M. Zhou, L. C. Yin, F. Li, H. M. Cheng, I. R. Gentle and G. Q. M. Lu, *J. Mater. Chem. A*, 2013, **1**, 9382-9394.
10.   X. L. Ji, K. T. Lee and L. F. Nazar, *Nat. Mater.*, 2009, **8**, 500-506.
11.   S. Evers and L. F. Nazar, *Accounts Chem. Res.*, 2013, **46**, 1135-1143.
12.   G. M. Zhou, L. C. Yin, D. W. Wang, L. Li, S. F. Pei, I. R. Gentle, F. Li and H. M. Cheng, *ACS Nano*, 2013, **7**, 5367-5375.
13.   M. Q. Zhao, Q. Zhang, J. Q. Huang, G. L. Tian, J. Q. Nie, H. J. Peng and F. Wei, *Nat. Commun.*, 2014, **5**, 3410.
14.   X. B. Cheng, J. Q. Huang, Q. Zhang, H. J. Peng, M. Q. Zhao and F. Wei, *Nano Energy*, 2014, **4**, 65-72.
15.   P. Simon and Y. Gogotsi, *Accounts Chem. Res.*, 2013, **46**, 1094-1103.
16.   Y. G. Zhang, Y. Zhao, A. Konarov, D. Gosselink, H. G. Soboleski and P. Chen, *J. Power Sources*, 2013, **241**, 517-521.
17.   Z. P. Chen, W. C. Ren, L. B. Gao, B. L. Liu, S. F. Pei and H. M. Cheng, *Nat. Mater.*, 2011, **10**, 424-428.
18.   H. Hu, Z. B. Zhao, W. B. Wan, Y. Gogotsi and J. S. Qiu, *Adv. Mater.*, 2013, **25**, 2219-2223.
19.   H. Y. Sun, Z. Xu and C. Gao, *Adv. Mater.*, 2013, **25**, 2554-2560.
20.   Y. Tao, D. B. Kong, C. Zhang, W. Lv, M. X. Wang, B. H. Li, Z. H. Huang, F. Y. Kang and Q. H. Yang, *Carbon*, 2014, **69**, 169-177.
21.   C. Zhang, W. Lv, W. G. Zhang, X. Y. Zheng, M. B. Wu, W. Wei, Y. Tao, Z. J. Li and Q. H. Yang, *Adv Energy Mater*, 2014, **4**, 1301565.
22.   W. Lv, Y. Tao, W. Ni, Z. Zhou, F. Y. Su, X. C. Chen, F. M. Jin and Q. H. Yang, *J. Mater. Chem.*, 2011, **21**, 12352-12357.
23.   W. F. Chen and L. F. Yan, *Nanoscale*, 2011, **3**, 3132-3137.
24.   Y. X. Xu, K. X. Sheng, C. Li and G. Q. Shi, *ACS Nano*, 2010, **4**, 4324-4330.
25.   L. Qiu, J. Z. Liu, S. L. Y. Chang, Y. Z. Wu and D. Li, *Nat. Commun.*, 2012, **3**, 1241.
26.   G. M. Zhou, S. F. Pei, L. Li, D. W. Wang, S. G. Wang, K. Huang, L. C. Yin, F. Li and H. M. Cheng, *Adv. Mater.*, 2014, **26**, 625-631.
27.   Q. Zeng, D.-W. Wang, K.-H. Wu, Y. Li, F. C. de Godoi and I. R. Gentle, *J. Mater. Chem. A*, 2014, **2**, 6439-6447.
28.   K. Morishige and N. Tateishi, *J. Chem. Phys.*, 2003, **119**, 2301-2306.
29.   Y. W. Zhu, S. Murali, M. D. Stoller, K. J. Ganesh, W. W. Cai, P. J. Ferreira, A. Pirkle, R. M. Wallace, K. A. Cychosz, M. Thommes, D. Su, E. A. Stach and R. S. Ruoff, *Science*, 2011, **332**, 1537-1541.
30.   C. G. Liu, Z. N. Yu, D. Neff, A. Zhamu and B. Z. Jang, *Nano Lett.*, 2010, **10**, 4863-4868.
31.   J. Kim, D. J. Lee, H. G. Jung, Y. K. Sun, J. Hassoun and B. Scrosati, *Adv. Funct. Mater.*, 2013, **23**, 1076-1080.
32.   D. W. Wang, G. M. Zhou, F. Li, K. H. Wu, G. Q. Lu, H. M. Cheng and I. R. Gentle, *Phys. Chem. Chem. Phys.*, 2012, **14**, 8703-8710.
33.   C. Zhang, W. Lv, X. Y. Xie, D. M. Tang, C. Liu and Q. H. Yang, *Carbon*, 2013, **62**, 11-24.
34.   Y. Yang, G. Y. Zheng and Y. Cui, *Chem. Soc. Rev.*, 2013, **42**, 3018-3032.
35.   J. Liu, T. Y. Yang, D. W. Wang, G. Q. M. Lu, D. Y. Zhao and S. Z. Qiao, *Nat. Commun.*, 2013, **4**, 2798.